Virtual Synchronous Control for Grid-Connected DFIG-Based Wind Turbines

Shuo Wang, *Student Member, IEEE*, Jiabing Hu, *Senior Member, IEEE*, and Xiaoming Yuan, *Senior Member, IEEE*

***Abstract*— This paper presents a virtual synchronous control (VSynC) for doubly fed induction generator (DFIG)-based wind turbines (WTs) to provide inertia contribution in particular when integrated into weak ac grid with low short-circuit ratio (SCR). Different from the traditional vector control (VC) based on the widely used phase-locked loop synchronizing technique, VSynC is capable of synchronizing DFIG with grid directly through the active power control. Damping control and current limitation are also designed to improve the stability and dynamic response of DFIG-based WT. Eigenvalue analysis shows that the VSynC-based DFIG displays pronounced superiority in stability to the typical VC based when connected to low-SCR ac grid. In such case, the power transfer capability of VSynC-based DFIG is not limited, which means the maximum theoretical power viz., 1 pu, can be achieved even when SCR is decreased to 1. By contrast, the maximum transmittable power of VC-based DFIG is highly restricted. Moreover, VSynC makes DFIG naturally provide the desired inertial response, and as a result enhances the grid frequency stability. Comparative study between the VSynC and the typical inertia control based on VC is also performed, and simulated results demonstrate the superior inertial response of VSynC-based DFIG attached to weak ac grid.**

***Index Terms*— Doubly fed induction generator (DFIG), inertial response, phase-locked loop (PLL), short-circuit ratio (SCR), stability, synchronization, virtual synchronous control (VSynC), weak grid, wind turbine (WT).**

NOMENCLATURE

$\boldsymbol{E}_{\mathrm{SG}}, \boldsymbol{E}_s$	Inner potential vectors of synchronous generator and doubly fed induction generator (DFIG).
$\delta_{\mathrm{sg}}, \delta_{\mathrm{dfig}}$	Power angles of SG and DFIG.
T_m, T_e	Mechanical and electromagnetic torques.
$\boldsymbol{U}_t, \boldsymbol{U}_s$	Vectors of terminal and infinite-bus voltages.
$\boldsymbol{I}_s, \boldsymbol{I}_r$	Stator and rotor current vectors.
$\boldsymbol{\Psi}_s, \boldsymbol{\Psi}_r$	Stator and rotor flux linkage vectors.
R_s, R_r	Stator and rotor resistances.
L_s, L_r	Stator and rotor self-inductances.
L_m	Mutual inductance.
ω_{base}	Angular frequency base value.
$\omega, \omega_1, \omega_0$	Inner potential, grid voltage, and rated angular frequencies in per unit.
U_r, θ_r	Magnitude and phase angle of rotor excitation voltage.

Manuscript received November 30, 2014; revised February 3, 2015; accepted March 9, 2015. Date of publication April 8, 2015; date of current version October 29, 2015. This work was supported in part by the National Basic Research Program (973 Program) of China under Grant 2012CB215100, in part by the National Natural Science of China for Excellent Young Scholars under Grant 51322704, in part by the Major Program of National Natural Science Foundation of China under Grant 51190104, and in part by the Program for New Century Excellent Talents in University through the Ministry of Education, China, under Grant NCET-12-0221. Recommended for publication by Associate Editor Riming Shao.

The authors are with the State Key Laboratory of Advanced Electromagnetic Engineering and Technology, School of Electrical and Electronic Engineering, Huazhong University of Science and Technology, Wuhan 430074, China (e-mail: wangshuo@hust.edu.cn; j.hu@hust.edu.cn; yuanxm@hust.edu.cn).

Color versions of one or more of the figures in this paper are available online at http://ieeexplore.ieee.org.

Digital Object Identifier 10.1109/JESTPE.2015.2418200

I. INTRODUCTION

WIND power will become an important power supply in China in the near future. By the example of the Jiuquan Wind Power Base in Gansu province, the installed wind capacity passed 10 GW by the end of 2014, which is expected to reach 30 GW by 2020. However, most of the wind farms are located ~1000-km away from the strong grid (Gansu power grid), which leads to the weak-grid integration of large-scale wind turbines (WTs). Such high penetration of wind power integrated into weak grid has presented multiple challenges to the secure and a stable operation of power grid [1], [2]. One of the prominent concerns regarding to the continuously rapid growth in penetration of wind power is its potential threat to future grid frequency stability, due to the irresponsibility of the installed WTs for disturbances on electromechanical time scale, i.e., large load fluctuations or generating unit losses, occurring frequently in power grid [2].

The effect of high penetration of renewable generation on system security, especially the frequency stability, is not unique in China. In 2009, EirGrid and SONI initiated a suite of studies entitled the facilitation of renewables, which is designed to examine the technical challenges with integrating significant volumes of wind farms into the power system of Ireland and Northern Ireland. A significant finding of the studies indicates that the integrity of the system following a frequency event is potentially compromised at instantaneously high penetrations of wind. The studies determine that the Transmission System Operators can securely manage the system provided that the system nonsynchronous penetration level in real-time operations remains <50%, due to the potentially falling of the average level of system inertia with increasing wind penetration [3]. The prediction for the 2030 GB generation mix shows that renewable generation, particularly the wind, has the most significant increase reaching 70.9 GW, driven by the U.K. government targets for renewable generation and greenhouse

gas emissions. A decrease in system inertia caused by large-scale integration of nonsynchronous generation would lead to increasing dynamic frequency response requirements to ensure system security [4], [5]. In addition, the results of studies that were specially designed to investigate the frequency responses of Western and Eastern Interconnections in the U.S. due to large-loss-generation events, under possible future system conditions with high levels of wind generation are reported in [6] and [7]. The results show the responsiveness of wind generation can improve the frequency response of grid.

In short, the capability of dynamic frequency support of wind power is urgently required in the near future to ensure that the system frequency stability is not compromised. In addition, the contributed inertia from wind power can further enhance the wind power permeability into grid.

As far as we know, there are two major categories of methods in the literature to implement the dynamic frequency support of wind power. One category can be considered as some modifications based on the typical vector control (VC) with the widely used phase-locked loop (PLL) synchronizing technique. For instance, in [8]–[13], some techniques, which are uniformly abbreviated as *df/dt* control here, are proposed to let WTs emulate inertia by providing an additional signal associated with the detected grid frequency differential signal to the torque or power reference to be tracked. However, PLL, which has since long been believed to be the precondition for any grid-connected voltage-source converter (VSC), might have negative impacts on system stability. From [14], it can be concluded that the increased PLL gains deteriorate the system stability. Hernefors *et al.* [15] suggests the bandwidth (BW) of PLLbe not larger than necessary. Furthermore, PLL technique makes the stable operation of the installed WTs rely on strong grid to some extent. When large-scale WTs are located in weak grid, power fluctuations may lead to an increase in magnitude and frequency variations in the grid voltage, which may adversely affect the performance of PLL and the control system thereof [16]–[18]. According to [19], the developed model behavior demonstrates that as short-circuit ratio (SCR) of the attached ac system is reduced, the resonances and nonlinearity due to the PLL and the ac filter behavior become more prominent, and potentially make the VSC more difficult to control. As a result, the maximum transmittable active power reduces with the decreasing SCR, down to 0.4 pu under the condition of SCR $= 1$. Meanwhile, the so-called frequency positive feedback in the converter system using the PLL technique under weak grid or islanding conditions is reported in [20]–[22]. Nevertheless, to the best of our knowledge, few, if any available, reports exist on reflecting the problems about the stability of DFIG-based WT with the typical PLL-based VC and its limited power transfer capability when connected to very weak ac system, which, as a matter of fact, would be largely influenced by the dynamic behavior of PLL. Furthermore, there are also no open reports about the corresponding response performance of VC-based DFIG with the typical inertia control aforementioned, i.e., *df/dt* control, when accessing a very weak ac system. These above-mentioned problems will constitute one of the main contributions in this paper.

The other category of methods can be uniformly summarized as the virtual synchronization. The concept of virtual synchronous generator (VSG) to add virtual rotational inertia to the nonsynchronous generators, i.e., wind power, photovoltaic, and so on, is proposed and put into practice in the European project VSYNC. The virtual inertia can be attained for any nonsynchronous generator by directly adding a short-term energy storage to it, combined with a suitable control mechanism for its power electronic interface to the grid. In this way, the generator can operate like a VSG, exhibiting some of the desired properties of SGs for short-time intervals and contributing to the stabilization of the grid frequency [23]–[26]. In addition, to overcome the difficulties associated with the PLL synchronizing technique for VSCs connected to weak ac grid, there is considerable tendency toward developing new control techniques to mimic the dynamic behavior of SGs due to the favorable performance of SGs in weak grid, which eliminates the need of PLL. In [17], a control method without utilizing PLL is proposed for HVdc system to maintain the stability when connected to weak ac grid, and also realize the black start for the restoration of power supply. Yuan *et al.* [18] propose a voltage-source control method making full-capacity WT generator synchronize with grid relying on its inner frequency produced by power imbalance, instead of the conventional current source control based on PLL. Zhang *et al.* [27] propose the so-called power synchronization control, which also makes a VSC terminal achieve an inherent synchronization with grid. Zhong and Weiss [28] develop the idea of operating an inverter as an SG called static synchronous generator by establishing a model of SG to cover all dynamics without any assumptions on the signals. The studies listed above are all aimed at the grid-connected VSCs. However, there are no available reports about DFIG-based WTs controlled with the concept of virtual synchronization to mimic the behavior of SG, and thus to provide the dynamic frequency support capability. This paper will present a virtual synchronous control (VSynC) method for DFIG-based WTs with reference to the well-known synchronization mechanism featured in SGs. The proposed VSynC makes DFIG-based WTs realize an inherent synchronization with grid, and more importantly, provide the desired inertial response naturally, which is the other contribution of this paper.

The remainder of this paper is organized as follows. In Section II, the principle and the implementation of VSynC for DFIG-based WT are illustrated. Section III presents the controller design and stability analysis with comparative studies between the proposed VSynC and the typical VC. In Section IV, the superior stability and dynamic frequency support capability of VSynC-based DFIG when connected to weak ac system are verified by simulation studies. Finally, the conclusions are drawn in Section V.

II. Virtual Synchronous Control for DFIG

A. Principle

To provide a better understanding of the proposed VSynC for DFIG-based WTs, this section first briefly summarizes the

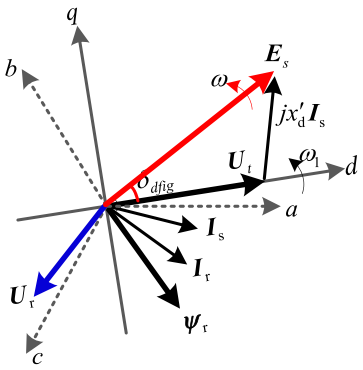

Fig. 1. Vector diagram of DFIG in the stator stationary reference frame under supersynchronous condition.

synchronization mechanism featured in SGs. In an SG, the inner potential vector is tightly connected to the rotor position.

Furthermore, the rotor dynamics are mainly determined by the interactions between mechanical and electromagnetic torques, which can be described by the well-known swing equation in generator mode as

$$T_m - T_e = \frac{J}{p}\frac{d\omega}{dt} \tag{1}$$

where p represents the pole pairs, ω is the electrical angular velocity, and also the angular frequency of the inner potential, T_m and T_e are the mechanical input and electromagnetic output torques, respectively. As a result, once SG is out of sync with grid during a transient, e.g., large load variations or generating unit losses occurring in grid, the resulting unbalanced torque applied on SG will automatically regulate the inner frequency ω until synchronization is achieved again. The kinetic energy released due to the speed regulation will undoubtedly provide temporary power support during the synchronization process.

On the other hand, with regard to the WT driven DFIG, Fig. 1 shows the vector diagram in the stator stationary reference frame under supersynchronous condition. The generator convention is adopted in the stator, while motor convention in the rotor. In Fig. 1, $\boldsymbol{E}_s$, which is defined as $\boldsymbol{E}_s = j(L_m/L_r)\boldsymbol{\Psi}_r$, represents the inner potential of DFIG's stator and the magnitude of $\boldsymbol{E}_s$ depends on that of the rotor flux $\boldsymbol{\Psi}_r$. The d-axis of the defined synchronous rotating reference frame is chosen to be aligned with the stator terminal voltage vector $\boldsymbol{U}_t$, and δ_{dfig} is defined as power angle, which is the electrical angle separating the two vectors $\boldsymbol{E}_s$ and $\boldsymbol{U}_t$. Because the inner potential $\boldsymbol{E}_s$ is always orthogonal to $\boldsymbol{\Psi}_r$, the angular frequency of $\boldsymbol{E}_s$, represented by ω to distinguish from the grid frequency ω_1, equals to that of $\boldsymbol{\Psi}_r$. While the angular velocity of rotor flux $\boldsymbol{\Psi}_r$ can be manipulated by the adjustment of the rotor excitation voltage, $\boldsymbol{U}_r$, determined by the rotor-side converter (RSC) control.

As a result, the rotational angular velocity of the rotor excitation voltage $\boldsymbol{U}_r$ can be regulated automatically when unbalanced power applied on DFIG occurs, which can meanwhile achieve the goal for regulating the inner frequency ω of $\boldsymbol{E}_s$ as mentioned above. Therefore, ω can be directly produced

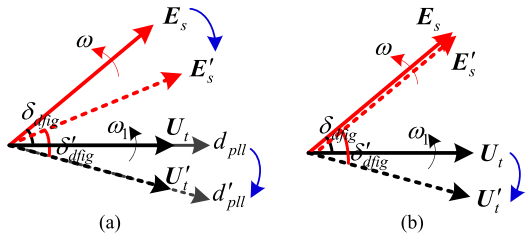

Fig. 2. Comparative responses of DFIG's stator inner potential between proposed (b) VSynC and (a) PLL-based synchronization methods.

by means of a virtual swing equation as

$$P_e^{\text{ref}} - P_e^{\text{meas}} = T_j \frac{d\omega}{dt} \tag{2}$$

where P_e^{ref} is the reference value of active power produced by the outer speed controller and P_e^{meas} represents the total output active power from both DFIG's stator and rotor. In addition, T_j represents the inherent inertia constant, and the role is similar to the inertia constant of SG, represented by H in general. The typical inertia constants for SGs of the large conventional power plants are in the range of 2–9 s, and the physical inertia constant of the modern large WT is more or less equal to the average of the conventional power plants [29]. In this paper, the inertia constant T_j is taken as 10, which means to mimic the inertial response behavior of SG with $H = 5$ s.

According to the idea aforementioned, the slip frequency ω_{slip} can be obtained by the difference between ω and ω_r, and the phase angle of the rotor excitation voltage, represented by θ_r, is further generated by the integral of the slip frequency as

$$\theta_r = \int (\omega - \omega_r)dt = \int \omega_{\text{slip}}\, dt \tag{3}$$

where ω_r is the electrical angular velocity of DFIG's rotor.

To provide comparisons between the proposed VSynC and the typical PLL-based VC, the dynamic characteristics on electromechanical time scale of the inner potential contained in WTs under the two methods are illustrated briefly through the vector diagrams, as shown in Fig. 2.

As shown in Fig. 2(a), the d_{pll} represents the rotating d-axis determined by the phase angle output from the PLL, which overlaps with the rotating space vector of grid voltage, $\boldsymbol{U}_t$, at steady state. The power angle, δ_{dfig}, is only determined by the control system. As a consequence, the position of WT's inner potential, $\boldsymbol{E}_s$, is synthetically determined by both the active power control loop and the PLL. The other variables with the superscript apostrophe are used to represent those after disturbance. When disturbance, e.g., sudden load increase, occurs in power grid, PLL will capture the change of phase angle and quickly trace the grid voltage vector. The inner potential also changes rapidly to $\boldsymbol{E}'_s$ based on the phase reference provided by PLL. As a result, the power angle almost has no change viz., $\delta'_{\text{dfig}} \approx \delta_{\text{dfig}}$. In short, the fast and precise response of PLL almost keeps the inner potential of WTs, $\boldsymbol{E}_s$, in sync with power grid all the time, which makes WTs almost immune to disturbances, and consequently behave

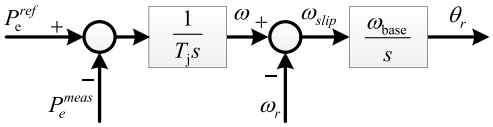

Fig. 3. Diagram of active power control.

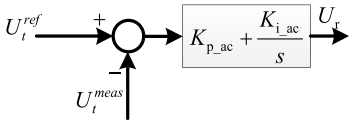

Fig. 4. Diagram of alternating-voltage control.

as a constant-power source with voltage amplitude variation neglected.

By contrast, the inner potential based on the proposed VSynC independently synchronizes with the power grid via the active power control on the basis of the power imbalance. As shown in Fig. 2(b), once disturbance occurs in power grid, which immediately causes an increase of power angle viz., $\delta'_{\text{dfig}} > \delta_{\text{dfig}}$, due to the independent frequency of inner potential $\boldsymbol{E}_s$, DFIG accordingly increases its output power to support the power shortage. Meanwhile, the power imbalance gradually causes the regulation of the angular frequency of the rotor excitation voltage by the active power control shown in (2) and (3), and further influences the inner potential to synchronize DFIG with the power grid until reaching equilibrium again. In this synchronization process, the rotor speed is also regulated due to the resulting unbalanced torques applied on DFIG, and the consequent release of the stored kinetic energy in the rotor results in an appreciable increase in output power over the first few seconds, which makes a positive contribution to the short-term frequency stability of power grid.

B. Implementation

This section describes the basic control structure of VSynC for DFIG-based WT, including active power control, alternating-voltage/reactive power control, supplementary damping control, and current limitation control.

1) Active Power and Alternating-Voltage/Reactive Power Controls: Active power control, as shown in Fig. 3, is the core control to ensure DFIG-based WT synchronize with the power grid without relying on PLL technique, which embodies the main idea described by (2) and (3). The power imbalance between the active power reference value and its actual output causes the regulation of ω via a virtual inertia unit until reaching a new equilibrium. The slip frequency ω_{slip} is obtained by the difference between ω and ω_r. The phase angle of the rotor excitation voltage is then obtained from the direct integral of the produced slip frequency.

The amplitude of DFIG's rotor excitation voltage can be directly produced by the alternating-voltage controller, as shown in Fig. 4, by referring to the excitation system of SG. In particular, in the case of weak grid, it is of vital importance for WTs to operate in the alternating-voltage control mode, which can provide the weak grid a certain degree of voltage support. While, if reactive power control

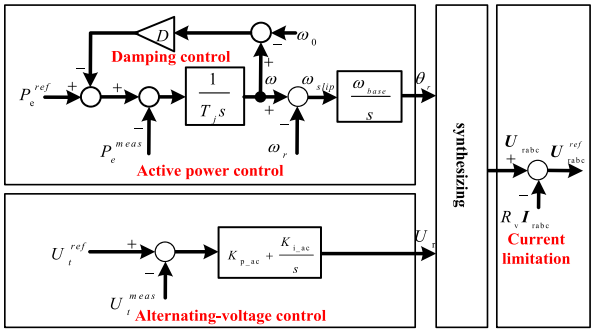

Fig. 5. Schematic of the proposed VSynC for DFIG-based WTs.

is required, the amplitude of rotor excitation voltage can also be produced directly by the reactive power controller. As a result, the required three-phase rotor excitation voltage can be directly synthesized from the generated phase angle and amplitude. The rotor excitation voltage vector $\boldsymbol{U}_{rabc}$ in rotor rotating reference frame can be given by

$$\boldsymbol{U}_{rabc} = \frac{2}{3}\left(U_{ra} + e^{j\frac{2}{3}\pi}U_{rb} + e^{j\frac{4}{3}\pi}U_{rc}\right) \tag{4}$$

where

$$\begin{aligned} U_{ra} &= U_r\cos(\theta_r) \\ U_{rb} &= U_r\cos(\theta_r - 2\pi/3) \\ U_{rc} &= U_r\cos(\theta_r - 4\pi/3). \end{aligned} \tag{5}$$

2) Supplementary Damping Control: It is clearly known that oscillations will occur in the rotor speed of SG following the disturbances on electromechanical time scale in power grid. These rotor oscillations give rise to the induced current in field and damper windings, which produces the damping torque in phase with the rotor speed especially in the damper windings. The same principle also applies to DFIG when adopting VSynC due to the resulting strong electromechanical coupling characteristic of the inner potential, which makes DFIG-based WT actively respond to disturbances in power grid. However, there is no damper winding in DFIG and resistances involved in both stator and rotor windings are very low. Therefore, supplementary damping control is necessitated to provide damping contribution to stabilize the DFIG-based WT. The damping power is produced by

$$P_D = D(\omega - \omega_1) \tag{6}$$

where D is the damping coefficient, and ω_1 is the measured grid frequency. ω_1 can also be the rated grid frequency, represented by ω_0 to distinguish it from grid frequency. ω_0 is used in this paper. P_D represents the damping power.

3) Current Limitation Control: In addition, a virtual resistance is suggested to effectively suppress the current transients due to the absence of inner current regulator. The control law is given by

$$\boldsymbol{U}_{rabc}^{\text{ref}} = \boldsymbol{U}_{rabc} - R_v\boldsymbol{I}_{rabc} \tag{7}$$

where R_v is the virtual resistance, $\boldsymbol{U}_{rabc}$ is the generated rotor excitation voltage by (4), and $\boldsymbol{U}_{rabc}^{\text{ref}}$ is the actual excitation voltage fed by RSC in rotor rotating reference frame. As a result, the entire control structure composed of

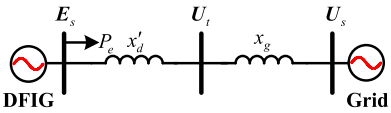

Fig. 6. Main circuit diagram of DFIG connected to an infinite-bus ac system.

active power control, alternating-voltage control, supplementary damping control, and current limitation control is shown in Fig. 5. Grid-side converter (GSC) control is still adopting the standard PLL-based method with typically cascaded control loops [30], which will be briefly explained in Sections III and IV.

III. Controller Design and Stability Analysis

A. Controller Design

Modeling of DFIG with VSynC connected to an infinite-bus ac system, as shown in Fig. 6, is built to study the influences of controller parameters and grid conditions on system performance, and to further design the system controllers theoretically. A weak ac system is typically characterized by the high impedance or low inertia. This section focuses only on the high impedance, which is described by the SCR according to [31]. Note that the speed and pitch angle controls with relatively slow dynamics are not considered temporarily in this section. A reduced-order DFIG model is first developed by considering the following conditions and assumptions [32].

1) The generator convention is adopted in the stator, while motor convention in the rotor.
2) The rate of change of stator flux linkage, $\boldsymbol{\Psi}_s$ is neglected.
3) The equations are derived in an ideally synchronous reference frame at constant speed ω_0, d-axis of which aligns with the terminal voltage vector, $\boldsymbol{U}_t$, at initial state.

The stator and rotor voltage equations for DFIG are given as

$$\boldsymbol{U}_t = -jx'_d\boldsymbol{I}_s + \boldsymbol{E}_s \tag{8}$$

$$\begin{cases} \dfrac{dE_{sd}}{dt} = -\dfrac{1}{T'_0}\left[E_{sd} - \left(x_d - x'_d\right)I_{sq}\right] + \omega_{\text{slip}}E_{sq} - \omega_{\text{base}}\dfrac{L_m}{L_r}U_{rq} \\ \dfrac{dE_{sq}}{dt} = -\dfrac{1}{T'_0}\left[E_{sq} + \left(x_d - x'_d\right)I_{sd}\right] - \omega_{\text{slip}}E_{sd} + \omega_{\text{base}}\dfrac{L_m}{L_r}U_{rd} \end{cases} \tag{9}$$

where

$$\begin{aligned} \boldsymbol{E}_s &= j\frac{L_m}{L_r}\boldsymbol{\Psi}_r, \quad x_d = L_s, \quad x'_d = L_s - \frac{L_m^2}{L_r} \\ T'_0 &= \frac{L_r}{(R_r + R_v)\omega_{\text{base}}} \end{aligned} \tag{10}$$

U_{rd} and U_{rq} are the d–q components of the generated rotor excitation voltage $\boldsymbol{U}_{rabc}$ by (4). All the quantities except slip frequency ω_{slip} and angular frequency base value ω_{base} are per-unit (pu) values.

Assume that the current injected into grid from GSC can be neglected relative to the stator current, and meanwhile, ignore the influence of GSC control so as to simplify the analysis. According to the main circuit shown in Fig. 6, there exist the following relationships:

$$I_{sd} = \frac{1}{X'}(E_{sq} - U_{sq}), \quad I_{sq} = -\frac{1}{X'}(E_{sd} - U_{sd}) \tag{11}$$

where

$$X' = x'_d + x_g. \tag{12}$$

Thus, a small-signal representation of (11) can be written as

$$\Delta I_{sd} = \frac{\Delta E_{sq}}{X'}, \quad \Delta I_{sq} = -\frac{\Delta E_{sd}}{X'}. \tag{13}$$

The d–q components of rotor excitation voltage vector, $\boldsymbol{U}_{rabc}$, can be represented as

$$U_{rd} = U_r\cos\theta_r, \quad U_{rq} = U_r\sin\theta_r. \tag{14}$$

If the operating points are denoted with subscript 0, the cosine and sine functions can be linearized as

$$\begin{cases} \Delta U_{rd} = \Delta U_r\cos\theta_{r0} - U_{r0}\sin\theta_{r0}\Delta\theta_r \\ \Delta U_{rq} = \Delta U_r\sin\theta_{r0} + U_{r0}\cos\theta_{r0}\Delta\theta_r. \end{cases} \tag{15}$$

Based on (13) and (15), the relationships of inner potential ΔE_{sd} and ΔE_{sq} versus the change of phase angle and a magnitude of the rotor excitation voltage is obtained by linearizing (9) as

$$\begin{cases} \Delta E_{sd} = G_{E_{sd}\theta_r}(s)\Delta\theta_r + G_{E_{sd}U_r}(s)\Delta U_r \\ \Delta E_{sq} = G_{E_{sq}\theta_r}(s)\Delta\theta_r + G_{E_{sq}U_r}(s)\Delta U_r \end{cases} \tag{16}$$

where

$$\begin{aligned} G_{E_{sd}\theta_r}(s) &= bU_{r0}\frac{\omega_{\text{slip0}}\sin\theta_{r0} - (a-s)\cos\theta_{r0}}{(\omega_{\text{slip0}})^2 + (a-s)^2} \\ G_{E_{sd}U_r}(s) &= -b\frac{\omega_{\text{slip0}}\cos\theta_{r0} + (a-s)\sin\theta_{r0}}{(\omega_{\text{slip0}})^2 + (a-s)^2} \\ G_{E_{sq}\theta_r}(s) &= -bU_{r0}\frac{\omega_{\text{slip0}}\cos\theta_{r0} + (a-s)\sin\theta_{r0}}{(\omega_{\text{slip0}})^2 + (a-s)^2} \\ G_{E_{sq}U_r}(s) &= b\frac{(a-s)\cos\theta_{r0} - \omega_{\text{slip0}}\sin\theta_{r0}}{(\omega_{\text{slip0}})^2 + (a-s)^2} \end{aligned} \tag{17}$$

and a, b, and X are defined as follows:

$$a = -\frac{1}{T'_0}\frac{X}{X'}, \quad b = -\omega_{\text{base}}\frac{L_m}{L_r}, \quad X = x_d + x_g. \tag{18}$$

The output active power can be approximately obtained by

$$P_e = \text{Re}\left[\boldsymbol{E}_s\cdot\boldsymbol{I}_s^*\right] \approx \text{Re}\left[\boldsymbol{U}_s\cdot\boldsymbol{I}_s^*\right]. \tag{19}$$

Thus, linearizing (19) yields

$$\Delta P_e \approx \frac{U_{sd0}}{X'}\Delta E_{sq} - \frac{U_{sq0}}{X'}\Delta E_{sd}. \tag{20}$$

In addition, due to the high impedance featured in weak ac system, the terminal voltage $\boldsymbol{U}_t$ has high sensitivity to the change of inner potential of DFIG. It is clear from Fig. 6 that

$$\boldsymbol{U}_t = \frac{x_g}{X'}\boldsymbol{E}_s + \frac{x'_d}{X'}\boldsymbol{U}_s \tag{21}$$

$$\Delta U_{td} = \frac{x_g}{X'}\Delta E_{sd}, \quad \Delta U_{tq} = \frac{x_g}{X'}\Delta E_{sq}. \tag{22}$$

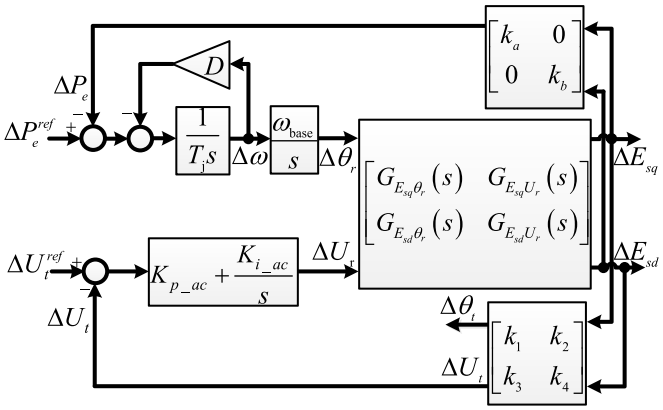

Fig. 7. Simplified small-signal mathematic model of VSynC-based DFIG connected to ac system.

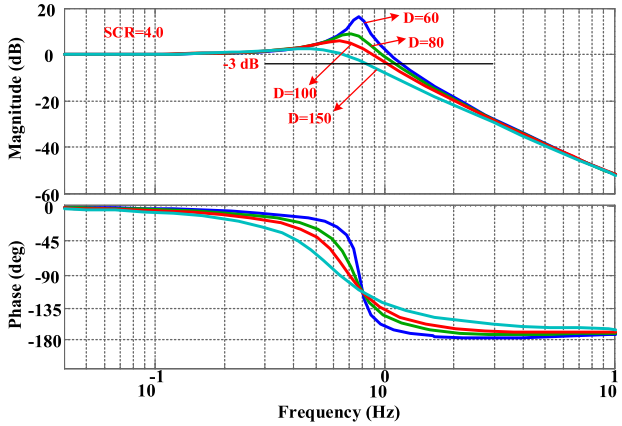

Fig. 8. Closed-loop bode diagrams of the active power control loop of DFIG with different damping coefficients.

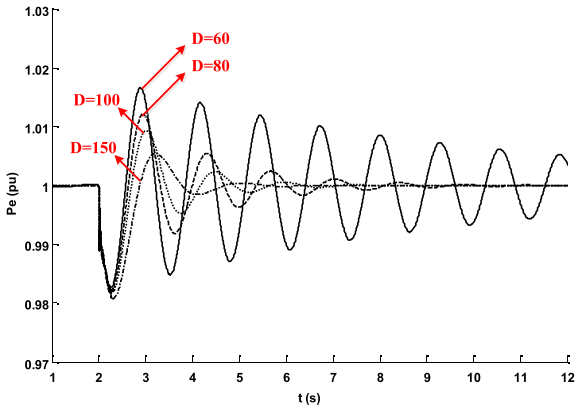

Fig. 9. Responses of DFIG's active power with different damping coefficients under the perturbation of a small phase step at the infinite source.

Similarly, the polar form is expressed as

$$\begin{cases} \Delta U_t = \dfrac{U_{td0}}{U_{t0}}\Delta U_{td} + \dfrac{U_{tq0}}{U_{t0}}\Delta U_{tq} \\ \Delta\theta_t = \dfrac{U_{td0}}{U_{t0}^2}\Delta U_{tq} - \dfrac{U_{tq0}}{U_{t0}^2}\Delta U_{td} \end{cases} \tag{23}$$

Finally, by substituting (22) in (23), the relationships of phase angle and a magnitude of the terminal voltage versus the inner potential of DFIG can be written as

$$\begin{cases} \Delta U_t = \dfrac{x_g}{X'}\left(\dfrac{U_{td0}}{U_{t0}}\Delta E_{sd} + \dfrac{U_{tq0}}{U_{t0}}\Delta E_{sq}\right) \\ \Delta\theta_t = \dfrac{x_g}{X'}\left(\dfrac{U_{td0}}{U_{t0}^2}\Delta E_{sq} - \dfrac{U_{tq0}}{U_{t0}^2}\Delta E_{sd}\right). \end{cases} \tag{24}$$

The simplified small-signal mathematic model of DFIG connected to a weak ac system is shown in Fig. 7, where the $k\_$ parameters are defined as

$$\begin{cases} k_a = \dfrac{U_{sd0}}{X'}, \quad k_b = -\dfrac{U_{sq0}}{X'} \\ k_1 = \dfrac{x_g}{X'}\dfrac{U_{td0}}{U_{t0}^2}, \quad k_2 = -\dfrac{x_g}{X'}\dfrac{U_{tq0}}{U_{t0}^2} \\ k_3 = \dfrac{x_g}{X'}\dfrac{U_{tq0}}{U_{t0}}, \quad k_4 = \dfrac{x_g}{X'}\dfrac{U_{td0}}{U_{t0}}. \end{cases} \tag{25}$$

As can be seen in Fig. 7, the stability of active power control and alternating-voltage control loops is affected synthetically by both of the controller parameters and grid conditions.

In general, the terminal voltage of each individual WT is stabilized via relatively fast inner voltage control. Referring to [11] and [33], the controller parameters in the WT-level voltage regulator are designed as $K_{p\_\mathrm{ac}} = 0$, $K_{i\_\mathrm{ac}} = 40$, respectively, and the corresponding BW is at about a few hertz. Therefore, the gains of the alternating-voltage controller in the proposed VSynC method are selected as normal in order to obtain similar dynamic response. The alternating-voltage controller parameters are set to $K_{p\_\mathrm{ac}} = 1$ and $K_{i\_\mathrm{ac}} = 40$, respectively. The parameters of DFIG, GSC controllers, and transmission line are given in Appendix A.

Active power control loop is specially chosen as the major studied object here because of its important role in synchronization functionality and inertial response performance for VSynC-based DFIG. However, it does not mean that the virtual synchronization method itself makes the appreciable inertial response characteristic appear, which is actually just a replacement for the PLL synchronizing technique due to the negative effects caused by PLL when accessing weak grid. The crucial factor determining whether the VSynC-based DFIG WTs provide the appreciable inertia support is the dynamic response speed of the active power control. Fast dynamic response of the active power control makes DFIG-based WT achieve synchronization with power grid very quickly when disturbance occurs, which means that the synchronization process is similar to the rapid synchronization characteristic of PLL. As a consequence, the inertial response capability is poor and not quite ideal. Therefore, the relative slow dynamic response of the active power control is the prerequisite for VSynC-based DFIG to provide the appreciable inertial response.

In this paper, the integration constant T_j is taken as 10 to mimic the dynamic behavior of SG with inertia constant $H = 5$ s, and the virtual resistance R_v is set as 1. Furthermore, the coefficient D has great influence on the dynamic response of active power control loop. Under the condition of DFIG operating at rated power level and SCR being 4, Fig. 8 shows the closed-loop bode diagrams for DFIG with different values of D. It can be clearly seen that there appears a big peak on the amplitude-frequency curve when D is set as 60, which dedicates an apparent oscillatory behavior with

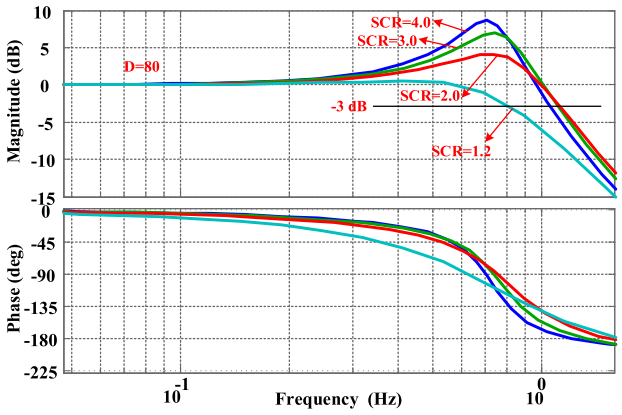

Fig. 10. Closed-loop bode diagrams of the active power control loop of DFIG under different ac-system SCR values.

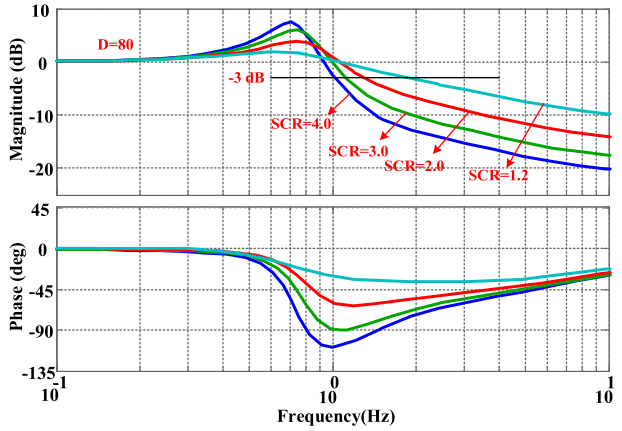

Fig. 11. Closed-loop bode diagrams of the alternating-voltage control loop of DFIG under different ac-system SCR values.

weak damp. With the increase of damping coefficient, the peak drops and the corresponding phase margin (at -3 dB roll-off point) increases gradually, which means the stability is improved. In addition, the increase of coefficient D makes the BW of the active power control loop reduced from 1.14 ($D = 60$) to 0.785 Hz ($D = 150$). Fig. 9 gives the corresponding DFIG active power responses with different damping coefficients under the perturbation of a small phase step at the infinite source, which is consistent with the results obtained from the bode diagram in Fig. 8.

In addition, the influences of ac-system SCR on stability of active power control and alternating-voltage control loops are also evaluated through bode diagrams. By taking the condition of $D = 80$ as an example, Fig. 10 indicates that DFIG with VSynC clearly presents enhanced stability as the ac system weakens and accordingly the BW of the active power control is reduced to 0.786 Hz under the SCR $= 1.2$. Furthermore, the influence of lower ac-system SCR on alternating-voltage control largely reflects the higher sensitivity of ac-voltage magnitude and phase angle to wind power fluctuations. As a consequence, the BW of alternating-voltage control loop shows the increasing tendency, which is from 1.02 Hz (SCR $= 4$) to $\sim$1.86 Hz (SCR $= 1.2$), as shown in Fig. 11.

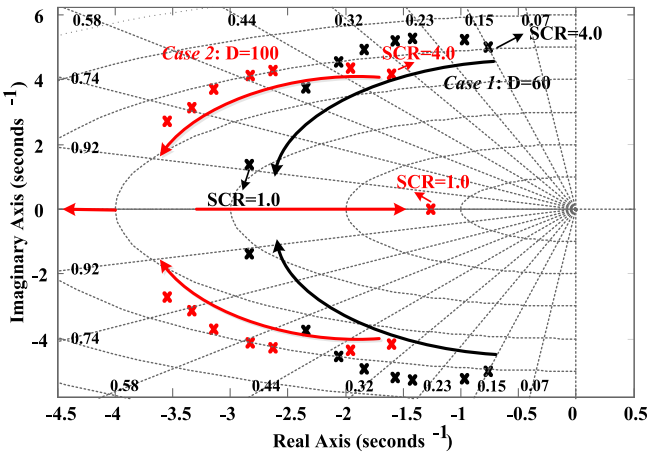

Fig. 12. Changes of network dominant eigenvalues for VSynC-based DFIG with different ac-system SCR and damping coefficients.

B. Stability Analysis

This section is to validate the results obtained from the bode diagrams aforementioned through eigenvalues analysis and also the comparative studies between the proposed VSynC and the typical VC are performed for DFIG connected to low-SCR ac system.

First, two cases of VSynC-based DFIG operating at rated power level with different damping coefficient values are studied. Relative to the base case (Case 1), where the damping coefficient D is taken as 60, Case 2 increases the damping coefficient to 100 with all the other parameters unchanged.

Fig. 12 shows the changes of system dominant eigenvalues in black and red, which are depicted as Case 1 and Case 2, respectively. It can be clearly seen that the system dominant eigenvalue pair in Case 1 gradually moves to left as the ac-system SCR decreases from 4 to 1, which means stronger damping and a more stable system. Fig. 12 also displays that the dominant eigenvalue pairs in red shift left compared with the black ones in Case 1, which indicates that the stability of DFIG system can be improved obviously when increasing the damping coefficient suitably. When SCR decreases to 1, the dominant eigenvalue pair in Case 2 finally moves on the negative real axis, which means no oscillations in this dominant mode occurs the following perturbations in grid.

In theory, under some assumptions, the SCR value imposes a theoretical limitation on the maximum power that DFIG can inject into the ac system due to the following relationship [34]:

$$P_e \approx \text{SCR} \cdot \sin\delta \leq \text{SCR} \tag{26}$$

where P_e represents the output power in pu, and δ is defined as the load angle between $\boldsymbol{U}_t$ and $\boldsymbol{U}_s$. In other words, for DFIG connected to a very low SCR system, e.g., SCR $= 1$, the maximum transmittable power is $P_e = 1$ pu. Therefore, it is well worth noting that the VSynC-based DFIG can achieve the maximum theoretical output power even under the condition of SCR $= 1$, and also shows excellent performance and good stability.

By comparison, the stability and active power transfer capability of the VC-based DFIG connected to low-SCR ac system is studied using the same infinite-bus ac system, as

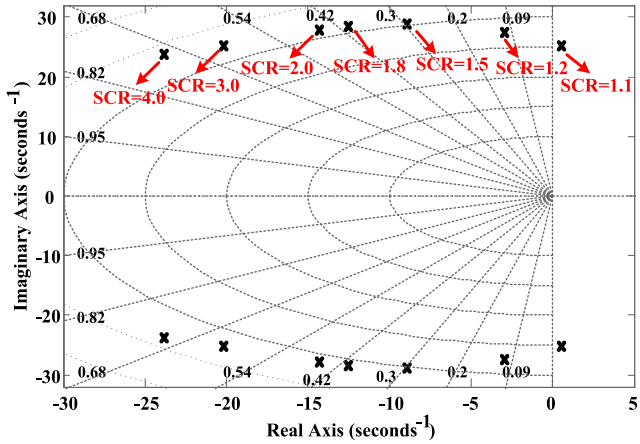

Fig. 13. Influence of ac-system SCR on the system dominant eigenvalues for VC-based DFIG when operating at rated power level.

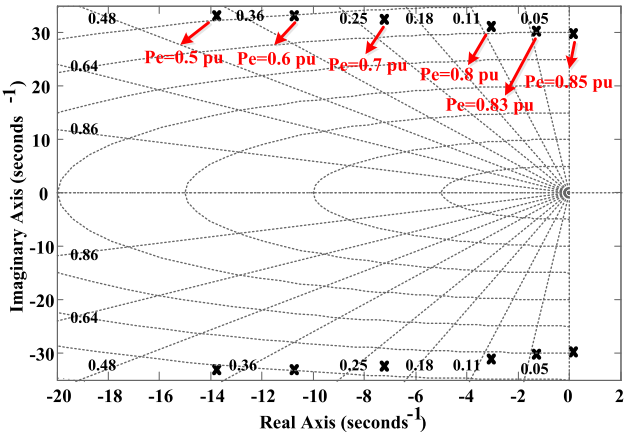

Fig. 14. Influence of delivering active power on the system dominant eigenvalues for VC-based DFIG under the condition of SCR = 1.

shown in Fig. 6. Similarly, the dynamics of outside speed and pitch angle controls are not considered temporarily. Typical stator-voltage-oriented VC is the selected object and the overall control structure refers to that in [35]. The design of RSC control is to achieve the desired active power and alternating voltage. The aim of GSC control is to maintain the dc-link capacitor voltage and to guarantee the converter operation with unity power factor. The VC parameters are also given in Appendix A.

Fig. 13 shows how the locations of the system dominant eigenvalues vary as the ac-system SCR is decreased from SCR = 4 to SCR = 1.1. As shown in Fig. 13, the system dominant eigenvalue pair moves toward the imaginary axis gradually as the ac-system SCR decreases, which means the stability becomes poor. It also indicates that the dominant eigenvalue pair has a positive real part when the ac-system SCR is decreased to SCR = 1.1, implying negative damping and a dynamically unstable system. In other words, the VC-based DFIG operating at rated power level under the given control parameters cannot be running stably when SCR is as low as 1. The maximum transmittable power of DFIG under SCR = 1 can be observed evidently from Fig. 14. It can be clearly seen that the maximum actual output power is

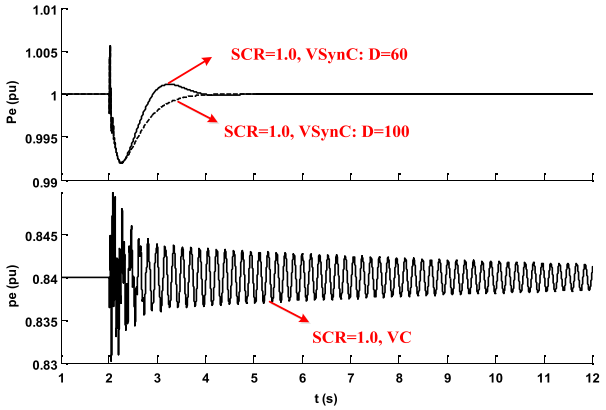

Fig. 15. Comparative results between VSynC and typical VC under the perturbation of a small phase step at the infinite source.

highly limited, approximately to 0.84 pu under the condition of SCR = 1.

Actually, according to the modal analysis, it can be concluded that the PLL is the primary participant of the dominant oscillation mode shown in Figs. 13 and 14, which means PLL dynamic behavior has a big impact on the stability of DFIG. More interestingly, the active power and alternating-voltage controls in RSC also have a significant boost in participation as the ac-system SCR decreases. In other words, there appear fairly strong interactions among the PLL, active power and alternating-voltage controls in RSC for VC-based DFIG connected to a very low SCR system, and the GSC control rarely affects the system stability, even in a very low-SCR ac system. This is because the transmitting power through GSC in DFIG system is much less than the power output from the stator, which directly leads to be a trivial matter compared with the grid-connected full-capacity converter systems, e.g., full-capacity converter WTs, VSC-HVdc, and so on. As a result, that is why the typical PLL-based VC method is still used for GSC control in the proposed VSynC method for RSC.

Time domain simulations are performed to briefly validate the results presented by the analysis above. As shown in Fig. 15, VC-based DFIG is almost operating at the most critical state when the output active power reaches 0.84 pu, and obviously, the VSynC-based DFIG shows superiority in system stability and power transfer capability under the condition of SCR = 1.

IV. Frequency Support Capability of DFIG-Based WTs With Virtual Synchronous Control

In addition to the superiority in stability of VSynC-based DFIG connected to low-SCR ac system, VSynC can also make DFIG naturally provide the appreciable inertial response to prevent the grid frequency from changing rapidly, which is the other important advantage worth mentioning. Simulations are carried out to demonstrate the capability of DFIG-based WTs with VSynC to positively contribute to stabilizing grid frequency when disturbance on electromechanical time scale, e.g., sudden connection of large loads, occurs in power grid.

The frequency support capability is verified by simulation studies on a nine-bus test system, as shown in Fig. 16, which

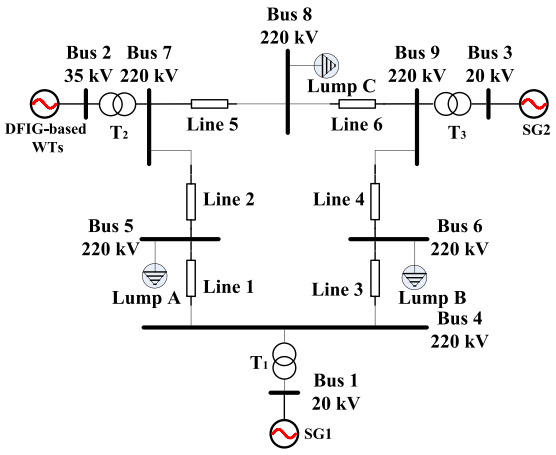

Fig. 16. Test system.

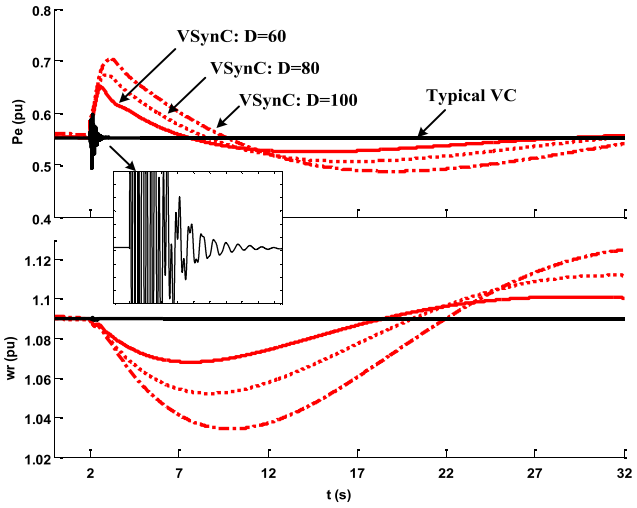

Fig. 17. Comparative responses to the abrupt load variation between the proposed VSynC with different damping coefficients and the typical VC without inertial control.

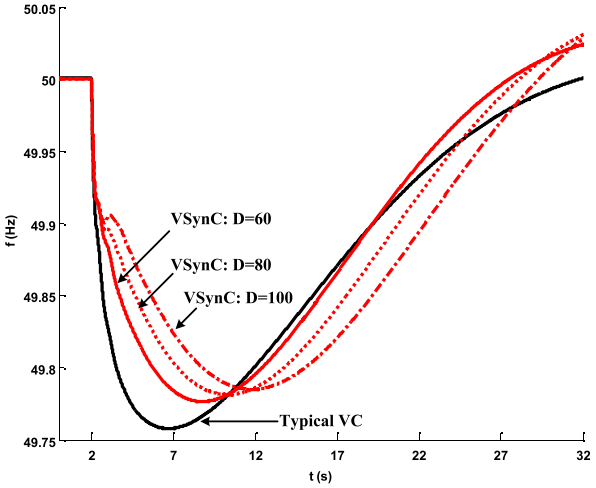

Fig. 18. System frequency responses between the proposed VSynC with different damping coefficients and the typical VC without inertial control.

consists of two conventional power plants (SG_1 and SG_2), three aggregated loads (Lump A, Lump B, and Lump C), and a DFIG-based wind farm rated at 600 MW (400 MW $\times$ 1.5 MW). Assume that a single DFIG-based WT represents the aggregate behavior of the whole wind farm. The conventional power plants SG_1 and SG_2 are rated at 1200 and 900 MW, respectively. The three loads, Lump A, Lump B, and Lump C, are 450, 250, and 300 MW, respectively. The turbine control strategy of DFIG is referring to GE 1.5-MW DFIG WT in [11]. Associated parameters of DFIG, SGs, and transmission lines are given in Appendixes A and B. The test system is designed specially as a quite low SCR system, which is approximately as low as 1.35 from the WTs' access point of view. In addition, the instantaneous penetration of wind power is reaching 33% initially. The following is divided into two parts. The first is to verify the frequency support capability of DFIG-based WTs with VSynC, in particular in the weak grid. In addition, by taking the typical *df/dt* control strategy [11] as an example, comparisons of the inertial responses between the proposed VSynC and the VC with typical *df/dt* control are performed.

A. Frequency Support Capability of DFIG-Based WTs With VSynC in Weak Grid

The initial wind velocity is fixed at 10 m/s (within Maximum Power Point Tracking area). There occurs a predefined disturbance by increasing Lump C from 300 to 500 MW at 2 s. Fig. 17 compares the responses to the abrupt load variation between the proposed VSynC and the typical VC without inertial control. It can be seen that the positive contribution of VSynC is noticeable. The DFIG-based WTs with typical VC can be viewed as a constant-power source for the disturbances on electromechanical time scale, and have no contribution to supporting the grid frequency. In addition, it is also worth noting that there exist serious oscillations, depicted in the inset of Fig. 17, which occur in the output power from VC-based DFIG, and are actually related with the dynamic behavior of PLL. On the contrary, the top waveforms in Fig. 17 clearly show that DFIG-based WTs with VSynC can positively provide an appreciable increase in output power to temporarily support the power shortage in grid for at least 5 s. In addition, the influence of damping coefficient on the response behavior can be observed clearly. The damping coefficient, D, in the three different cases is taken as 60, 80, and 100, respectively. The results show that the maximum value of overproduction power gradually increases from $\sim$12% to 15% of the rated power as the damping coefficient gets higher. Furthermore, the overproduction period grows in which WTs provide the extra power output until reaching the normal production power before disturbance.

Fig. 18 displays the system frequency responses for DFIG-based WTs with VSynC and typical VC. It is evident that the rate of change of the system frequency decreases significantly as the control BW reduces due to the increased damping coefficient, and meanwhile the minimum frequency point is improved. In above, as we can see from Figs. 17 and 18, VSynC presents good stability in low SCR ac system, and moreover, excellent frequency supporting capability.

In addition, though the increase of coefficient D can improve the system stability and enhance the inertial response

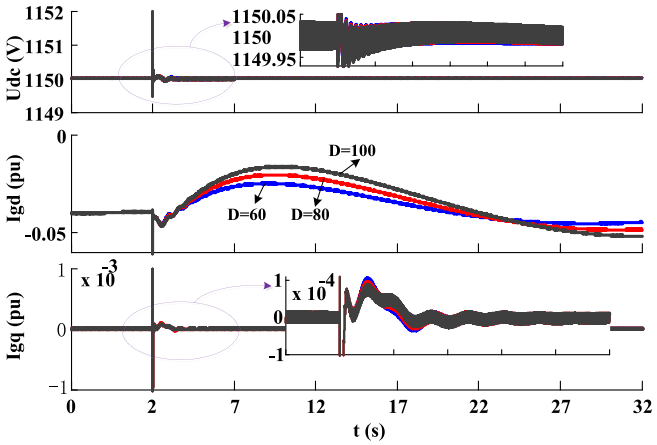

Fig. 19. Dynamic responses of GSC ac currents and dc-link voltage when VSynC is adopted for RSC when different damping coefficients.

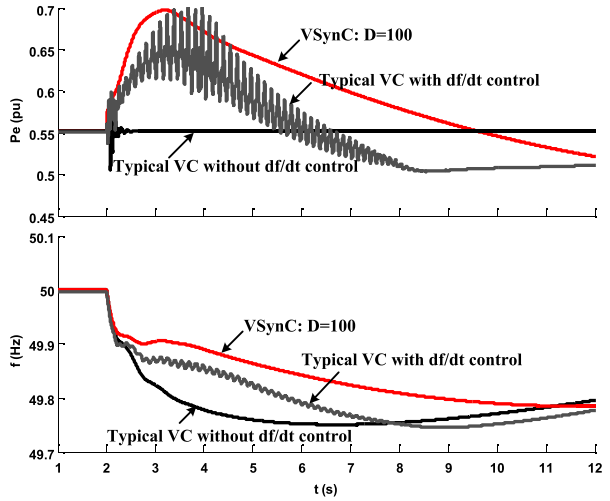

Fig. 20. Comparative responses between the proposed VSynC and the typical VC with *df/dt* control.

mentioned above, too large value of the coefficient D in active power control may severely deteriorate the dynamic response of the outer speed control loop and thus cause serious speed and power oscillations. In addition, the inertial response must be consequently limited when the initial wind speed or rotor speed is very low due to the minimum speed limit and also the risk of rotor stall. Under this condition, the inertial response can be limited by modifying the control parameters (T_j and D) to quicken the dynamic response of the active power control loop.

In addition, the dynamic responses of the GSC current represented by I_{gd} and I_{gq}, and the dc-link voltage, $U_{\rm dc}$, are also provided below under different values of coefficient D. From Fig. 19, it can be seen that the proposed VSynC almost has no impacts on the GSC current and dc-link voltage dynamics. This is because the dynamic response speeds of the dc-link voltage and current are designed as fast as normal.

B. Comparisons With VC-Based df/dt Control in Weak Grid

In addition, a comparative study between the proposed VSynC and the typical VC with *df/dt* control is performed using the same test system. The parameters of the *df/dt* control are given in Appendix B. As shown in Fig. 20, the response performance of DFIG with the typical VC-based *df/dt* control is badly affected in the weak grid. This is because that the output of PLL is used as the phase reference of the overall control system, and also the input signal of the *df/dt* control. Furthermore, the stability of PLL becomes poor as the grid weakens, and thus affects the response performance of DFIG-based WT. This section embodies the superiority of the VSynC-based DFIG on stability and dynamic frequency support capability when connected to a very weak ac grid.

TABLE I
DFIG PARAMETERS

Symbol	Description	value
$R_{\rm s}$	Stator resistance	0.023 pu
$R_{\rm r}$	Rotor resistance	0.016 pu
$L_{\rm s}$	Stator self-inductance	3.08 pu
$L_{\rm r}$	Rotor self-inductance	3.06 pu
$L_{\rm m}$	Mutual inductance	2.9 pu
$P_{\rm N}$	Rated power	1.5 MW
$U_{\rm N}$	Rated voltage	690 V
$f_{\rm N}$	Rated frequency	50 Hz
$P_{\rm base}$	System power base value	1.5 MW
$U_{\rm base}$	Voltage base value	690 V
$\omega_{\rm base}$	Frequency base value	100π

TABLE II
NETWORK CONFIGURATION PARAMETERS

Symbol	Description	value
$R_{\rm f}$	Filter resistance (GSC)	0.003 pu
$L_{\rm f}$	Filter inductance (GSC)	0.3 pu
C	DC capacitor	10000 μF
$U_{\rm dc}$	DC voltage	1150 V
$x_{\rm g}(L_{\rm g})$	Transmission line impedance	$L_{\rm g}$: 1/SCR mH
$U_{\rm s}$	Infinite-bus voltage	690 V

V. CONCLUSION

VSynC is presented for DFIG-based WTs referring to the well-known synchronization mechanism featured in SGs, which enables DFIG-based WT synchronize with power grid relying on the active power control, rather than the widely used PLL technique. Two major features of VSynC are elaborated throughout this paper and can be summarized as follows.

A. Superior Stability in Weak AC Grid

Theoretical analysis and simulation results show that the VSynC-based DFIG displays superiority in stability especially when connected to relatively low-SCR ac system. Accordingly, the power transfer capability of DFIG with VSynC is not limited, which means the maximum transmittable power viz., the rated power can be achieved even when SCR is decreased to 1. However, the stability of the typical VC-based DFIG will get dramatically worse as the ac-system SCR decreases, which is closely related to dynamic behavior of PLL. As a consequence, the maximum transmittable power of VC-based DFIG is highly limited, approximately down to 0.84 pu. Therefore, VSynC may be of great potential for DFIG-based

TABLE III
VSynC PARAMETERS

Symbol	Description	value
T_j	Integration constant	10
D	Damping coefficient	60, 80, 100, 150
R_v	Virtual resistance	1
K_{p_ac}, K_{i_ac}	Alternating-voltage controller	1, 40
K_{p_dc}, K_{i_dc}	DC voltage controller (GSC)	8, 400
K_{p_I}, K_{i_I}	Current controller (GSC)	0.83, 5
K_{p_pll},K_{i_pll}	PLL parameters (GSC)	60, 1400

TABLE IV
VC PARAMETERS

Symbol	Description	value
K_{p_P}, K_{i_P}	Active power controller (RSC)	1, 100
K_{p_ac}, K_{i_ac}	Alternating-voltage controller(RSC)	1, 40
K_{p_I1}, K_{i_I1}	Current controller (RSC)	0.6, 8
K_{p_dc}, K_{i_dc}	DC voltage controller (GSC)	8, 400
K_{p_I2}, K_{i_I2}	Current controller (GSC)	0.83, 5
K_{p_pll},K_{i_pll}	PLL parameters (RSC,GSC)	60, 1400

TABLE V
TURBINE CONTROL PARAMETERS OF DFIG

Symbol	Description	value
K_{p_v}, K_{i_v}	Speed controller	3, 0.6
K_p, K_i	Pitch angle controller	3, 30
P_{max}, P_{min}	Pitch angle limit	27, 0 deg
$\pm P_{rate}$	Pitch angle rate limit	±10 deg/s

TABLE VI
VC-BASED *df/dt* CONTROL PARAMETERS

Symbol	Description	value
T_f	Filter time constant	0.5 s
T_w	Washout filter time constant	6 s
K_p	Proportional coefficient	60

WTs in the weak grid applications. It is worth pointing out the result is obtained from a single-machine infinite-bus ac system under the specified control parameters given in this paper, but without considering any amplitude limiter actions, feed-forward and feedback decoupling items, converters' and DFIG's capacity problems.

B. Superior Dynamic Frequency Support Capability

A three-machine test system is used to demonstrate the dynamic frequency support capability of the VSynC-based DFIG. Note that the access point of DFIG-based WTs is relatively weak and the ac-system SCR is designed as low as 1.35 from the WTs' assess point of view. According to the simulated results, VSynC shows good stability in low SCR ac system, and more importantly, enables DFIG-based WT to naturally provide the desired inertial response following disturbance and thus to present the excellent dynamic frequency support capability. Comparative studies between the proposed VSynC and the typical VC-based *df/dt* control show that the response of DFIG with VC-based *df/dt* control is seriously affected, which is actually associated with the dynamic behavior of PLL when operating in weak ac system.

TABLE VII
SG_1 AND SG_2 PARAMETERS

Symbol	SG1	SG2
X_d	2	2.13
X'_d	0.35	0.308
X''_d	0.252	0.234
X_q	2.19	2.07
X''_q	0.243	0.234
R_s	0.0045	0.005
X_l	0.117	0.117
T'_{d0}	8	6.09
T''_{d0}	0.0681	0.033
T''_{q0}	0.9	0.029
H	5.2 s	3.84 s
pole pairs (p)	1	1
P_N	1200 MW	900 MW
U_N	20 kV	20 kV
f_N	50 Hz	50 Hz

TABLE VIII
NETWORK CONFIGURATION PARAMETERS

(S_b=1200MW, U_b=220* $\overline{2\ 3}$ kV)

Symbol	Transmission line
Line 1	0.6621 pu
Line 2	1.9862 pu
Line 3	0.6621 pu
Line 4	0.6621 pu
Line 5	1.9862 pu
Line 6	0.6621 pu

APPENDIX A

See Tables I–IV.

APPENDIX B

See Tables V–VIII.

REFERENCES

[1] R. Piwko, N. Miller, J. Sanchez-Gasca, X. Yuan, R. Dai, and J. Lyons, "Integrating large wind farms into weak power grids with long transmission lines," in *Proc. CES/IEEE 5th Int. Power Electron. Motion Control Conf. (IPEMC)*, Aug. 2006, pp. 1–7.

[2] X. Yuan, S. Cheng, and J. Wen, "Prospects analysis of energy storage application in grid integration of large-scale wind power," *Autom. Electr. Power Syst.*, vol. 37, no. 1, pp. 14–18, Jan. 2013.

[3] *Ensuring a Secure, Reliable and Efficient Power System in a Changing Environment*, EirGrid, Dublin, Ireland, 2011.

[4] National Grid. (Sep. 2012). *UK Future Energy Scenarios*. [Online]. Available: http://www.nationalgrid.com/NR/rdonlyres/332FFA28-6900-4214-92BB-D3AD4FA5DC01/56611/UK_Future_Energy_Scenarios_2012.pdf

[5] A. Walden. (2014). *Future Balancing Services Requirements: Response*. [Online]. Available: http://www.nationalgrid.com/NR/rdonlyres/0F82BB0B-98E9-4B02-A514-3C87A85E60D8/42696/Future_Balancing_Services_Requirements_Response1.pdf

[6] U.S. Department of Energy. (2013). *Eastern Frequency Response Study*. [Online]. Available: http://www.osti.gov/servlets/purl/1083365/

[7] N. Miller, C. Loutan, M. Shao, and K. Clark, "Emergency response: U.S. system frequency with high wind penetration," *IEEE Power Energy Mag.*, vol. 11, no. 6, pp. 63–71, Nov./Dec. 2013.

[8] J. Ekanayake and N. Jenkins, "Comparison of the response of doubly fed and fixed-speed induction generator wind turbines to changes in network frequency," *IEEE Trans. Energy Convers.*, vol. 19, no. 4, pp. 800–802, Dec. 2004.

[9] F. M. Hughes, O. Anaya-Lara, N. Jenkins, and G. Strbac, "Control of DFIG-based wind generation for power network support," *IEEE Trans. Power Syst.*, vol. 20, no. 4, pp. 1958–1966, Nov. 2005.

[10] O. Anaya-Lara, F. M. Hughes, N. Jenkins, and G. Strbac, "Contribution of DFIG-based wind farms to power system short-term frequency regulation," *IEE Proc.-Generat., Transmiss. Distrib.*, vol. 153, no. 2, pp. 164–170, Mar. 2006.

[11] K. Clark, N. W. Miller, and J. J. Sanchez-Gasca. (2010). "Modeling of GE wind turbine generators for grid studies," GE-Power Systems Energy Consulting, General Electric International, Inc., Schenectady, NY, USA, Tech. Rep. 112. [Online]. Available: http://www.gepower.com/prod_serv/Products/utilitysoftware/en/downloads/09100_Modeling_of_Ge_Wind_Turbine_ Generators_for_Grid_Studies.pdf

[12] J. Morren, S. W. H. de Haan, W. L. Kling, and J. A. Ferreira, "Wind turbines emulating inertia and supporting primary frequency control," *IEEE Trans. Power Syst.*, vol. 21, no. 1, pp. 433–434, Feb. 2006.

[13] Ö. Göksu, R. Teodorescu, P. Rodriguez, and L. Helle, "A review of the state ofthe art in control of variable-speed wind turbines," in *Proc. 9th Int. Workshop Large-Scale Integr. Wind Power Power Syst.*, QC, Canada, Oct. 2010.

[14] D. Jovcic, L. A. Lamont, and L. Xu, "VSC transmission model for analytical studies," in *Proc. IEEE Power Eng. Soc. General Meeting*, vol. 3. Toronto, ON, Canada, Jul. 2003, pp. 1737–1742.

[15] L. Harnefors, M. Bongiorno, and S. Lundberg, "Input-admittance calculation and shaping for controlled voltage-source converters," *IEEE Trans. Ind. Electron.*, vol. 54, no. 6, pp. 3323–3334, Dec. 2007.

[16] T. Midtsund, J. A. Suul, and T. Undeland, "Evaluation of current controller performance and stability for voltage source converters connected to a weak grid," in *Proc. 2nd IEEE Int. Symp. Power Electron. Distrib. Generat. Syst. (PEDG)*, Jun. 2010, pp. 382–388.

[17] Y. Jiang-Häfner and Ludvika, "HVDC system and method to control a voltage source converter in a HVDC system," U.S. Patent 2009 0 279 328 A1, Nov. 12, 2009.

[18] X. Yuan, A. M. Ritter, H. Weng, and R. W. Delmerico, "System and method for control of a grid connected power generating system," U.S. Patent 2010 0 142 237 A1, Jun. 10, 2010.

[19] M. Durrant, H. Werner, and K. Abbott, "Model of a VSC HVDC terminal attached to a weak AC system," in *Proc. IEEE Conf. Control Appl.*, Istanbul, Turkey, Jun. 2003, pp. 178–182.

[20] D. Dong, J. Li, D. Boroyevich, P. Mattavelli, I. Cvetkovic, and Y. Xue, "Frequency behavior and its stability of grid-interface converter in distributed generation systems," in *Proc. 27th IEEE Appl. Power Electron. Conf. Expo.*, Orlando, FL, USA, Feb. 2012, pp. 1887–1893.

[21] X. Wang and W. Freitas, "Impact of positive-feedback anti-islanding methods on small-signal stability of inverter-based distributed generation," *IEEE Trans. Energy Convers.*, vol. 23, no. 3, pp. 923–931, Sep. 2008.

[22] P. Du, Z. Ye, E. E. Aponte, J. K. Nelson, and L. Fan, "Positive-feedback-based active anti-islanding schemes for inverter-based distributed generators: Basic principle, design guideline and performance analysis," *IEEE Trans. Power Electron.*, vol. 25, no. 12, pp. 2941–2948, Dec. 2010.

[23] J. Driesen and K. Visscher, "Virtual synchronous generators," in *Proc. IEEE Convers. Del. Elect. Energy 21st Century Power Energy Soc. General Meeting*, Jul. 2008, pp. 1–3.

[24] T. V. Van *et al.*, "Virtual synchronous generator: An element of future grids," in *Proc. IEEE PES Innov. Smart Grid Technol. Conf. Eur.*, Oct. 2010, pp. 1–7.

[25] K. Visscher and S. W. H. de Haan, "Virtual synchronous machines (VSG's) for frequency stabilisation in future grids with a significant share of decentralized generation," in *Proc. CIRED Seminar SmartGrids Distrib. (IET-CIRED)*, Jun. 2008, pp. 1–4.

[26] M. P. N. van Wesenbeeck, S. W. H. de Haan, P. Varela, and K. Visscher, "Grid tied converter with virtual kinetic storage," in *Proc. IEEE Bucharest PowerTech Conf.*, Jun./Jul. 2009, pp. 1–7.

[27] L. Zhang, L. Harnefors, and H.-P. Nee, "Power-synchronization control of grid-connected voltage-source converters," *IEEE Trans. Power Syst.*, vol. 25, no. 2, pp. 809–820, May 2010.

[28] Q.-C. Zhong and G. Weiss, "Static synchronous generators for distributed generation and renewable energy," in *Proc. IEEE/PES Power Syst. Conf. Expo.*, Mar. 2009, pp. 1–6.

[29] J. Morren, J. Pierik, and S. W. H. de Haan, "Inertial response of variable speed wind turbines," *Electr. Power Syst. Res.*, vol. 76, no. 11, pp. 980–987, 2006.

[30] R. Pena, J. C. Clare, and G. M. Asher, "Doubly fed induction generator using back-to-back PWM converters and its application to variable-speed wind-energy generation," in *Proc. IEE Proc.-Elect. Power Appl.*, vol. 143, no. 3, pp. 231–241, May 1996.

[31] *Guide For Planning DC Links Terminating AC System Locations Having Low Short Circuit Capacities*, document CIGRE WG BI4.07, IEEE WGI5.05.05, 1997, pp. 149–152.

[32] J. B. Ekanayake, L. Holdsworth, and N. Jenkins, "Comparison of 5th order and 3rd order machine models for doubly fed induction generator (DFIG) wind turbines," *Electr. Power Syst. Res.*, vol. 67, no. 3, pp. 207–215, Dec. 2003.

[33] WECC Renewable Energy Modeling Task Force. (2010). *WECC Wind Power Plant Dynamic Modeling Guide*. [Online]. Available: http://renew-ne.org/wp-content/uploads/2012/05/WECCWindPlantDynamicModelingGuide.pdf

[34] L. Zhang, L. Harnefors, and H.-P. Nee, "Interconnection of two very weak AC systems by VSC-HVDC links using power-synchronization control," *IEEE Trans. Power Syst.*, vol. 26, no. 1, pp. 344–355, Feb. 2011.

[35] A. D. Hansen, P. Sørensen, F. Iov, and F. Blaabjerg, "Centralised power control of wind farm with doubly fed induction generators," *Renew. Energy*, vol. 31, no. 7, pp. 935–951, Jun. 2006.

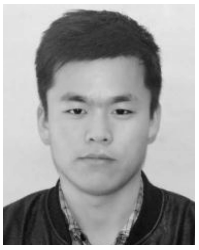

Shuo Wang (S'14) was born in Kaifeng, China, in 1990. He received the B.Eng. degree from the School of Electrical Engineering and Automation, Harbin Institute of Technology, Harbin, China, in 2011. He is currently pursuing the Ph.D. degree with the State Key Laboratory of Advanced Electromagnetic Engineering and Technology and the School of Electrical and Electronic Engineering, Huazhong University of Science and Technology, Wuhan, China.

His current research interests include control and stability analysis of grid-integrated wind turbines, in particular, on virtual synchronous control and optimized frequency response dynamics of grid-connected doubly fed induction generator-based wind turbines.

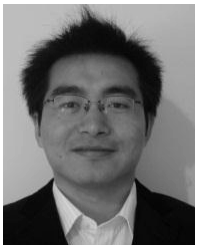

Jiabing Hu (S'05–M'10–SM'12) received the B.Eng. and Ph.D. degrees from the College of Electrical Engineering, Zhejiang University, Hangzhou, China, in 2004 and 2009, respectively.

He was a Visiting Scholar with the Department of Electronic and Electrical Engineering, University of Strathclyde, Glasgow, U.K., funded by the Chinese Scholarship Council, from 2007 to 2008. From 2010 to 2011, he was a Post-Doctoral Research Associate with the Sheffield Siemens Wind Power Research Center, and the Department of Electronic and Electrical Engineering, University of Sheffield, Sheffield, U.K. Since 2011, he has been a Professor with the State Key Laboratory of Advanced Electromagnetic Engineering and Technology, and the School of Electrical and Electronic Engineering, Huazhong University of Science and Technology, Wuhan, China. He has authored or co-authored over 70 peer-reviewed technical papers and one monograph entitled *Control and Operation of Grid-Connected Doubly-Fed Induction Generators*, and holds more than 20 issued/pending patents. His current research interests include grid-integration of large-scale renewables, modular multilevel converter for HVdc applications, and transient analysis and control of semiconducting power systems.

Dr. Hu was a recipient of the TOP TEN Excellent Young Staff Award from the Huazhong University of Science and Technology in 2014. He is supported by the National Natural Science of China for Excellent Young Scholars and the Program for New Century Excellent Talents in University from the Chinese Ministry of Education. He serves as a Domestic Member of the Editorial Board of *Frontiers of Information Technology and Electronic Engineering*.

Xiaoming Yuan (S'97–M'99–SM'01) received the B.Eng. degree from Shandong University, Jinan, China, in 1986, the M.Eng. degree from Zhejiang University, Hangzhou, China, in 1993, and the Ph.D. degree from the Federal University of Santa Catarina, Florianópolis, Brazil, in 1998, all in electrical engineering.

He was with Qilu Petrochemical Corporation, Zibo, China, from 1986 to 1990, where he was involved in the commissioning and testing of relaying and automation devices in power systems, adjustable speed drives, and high-power Uninterruptible Power Supply/System systems. From 1998 to 2001, he was a Project Engineer with the Swiss Federal Institute of Technology Zurich, Switzerland, where he was involved in flexible ac transmission systems and power quality. From 2001 to 2008, he was with the GE Global Research Center, Shanghai, China, as the Manager of the Low Power Electronics Laboratory. From 2008 to 2010, he was with the GE Global Research Center, Niskayuna, NY, USA, as an Electrical Chief Engineer. His current research interests include stability and control of power system with multimachines and multiconverters, control and grid-integration of renewable energy generations, and control of high voltage dc transmission systems.

Dr. Yuan was a recipient of the first prize paper award from the Industrial Power Converter Committee of the IEEE Industry Applications Society in 1999. He is a Distinguished Expert of the National Thousand Talents Program of China, and the Chief Scientist of the National Basic Research Program of China (973 Program).